Polymer Testing 137 (2024) 108531

Contents lists available at ScienceDirect

Polymer Testing

journal homepage: www.elsevier.com/locate/polytest

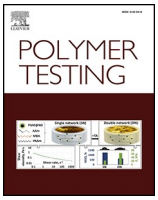

Understanding the shape-memory mechanism of thermoplastic polyurethane by investigating the phase-separated morphology: A dissipative particle dynamics study

Sungwoo Park [a], Jeong-ha Lee [b], Maenghyo Cho [a,c], Yun Seog Lee [a,c], Hayoung Chung [d], Seunghwa Yang [e,*]

[a] Department of Mechanical and Aerospace Engineering, Republic of Korea Institute of Advanced Machines and Design, Seoul National University, Seoul, Republic of Korea
[b] Department of Materials Science & NanoEngineering, Rice University, Houston, TX, United States
[c] Institute of Advanced Machines and Design, Seoul National University, Seoul, Republic of Korea
[d] Department of Mechanical Engineering, Ulsan National Institute of Science and Technology (UNIST), Ulsan, 44919, Republic of Korea
[e] Mechanical Engineering Division, School of Energy Systems Engineering, Chung-Ang University, 84 Heukseok-Ro, Dongjak-Gu, Seoul, 06974, Republic of Korea

ARTICLE INFO

Keywords:
Shape-memory polyurethane
Phase separation
Dissipative particle dynamics
Mesoscale simulation
Solubility parameter
Phase morphology
Shape-memory mechanism

ABSTRACT

Shape-memory polyurethanes (SMPUs) are promising materials that change shape in response to external heat. These polymers have a dual-segment structure: a hard segment for netpoint and a soft segment for molecular switch. Understanding the molecular behavior of each segment and microphase-separated morphology is crucial for comprehending the shape-memory mechanism. This study aimed to understand the shape-memory behavior by observing the phase separation of SMPU using mesoscale models based on dissipative particle dynamics (DPD) simulations. The SMPU copolymer was modeled using 4,4′-diphenylmethane diisocyanate (MDI, hard segment) and poly(ethylene oxide) (PEO, soft segment). By calculating segment solubility and repulsion parameters, we found that the hard-segment domain changes from isolated form to a lamellar and interconnected structure and eventually to a continuous form as its content increases. Combining these insights with shape-memory performance models can enhance our understanding of better SMPU design and contribute significantly to the optimization of smart stimuli-responsive materials.

1. Introduction

Smart materials known as shape-memory polymers (SMPs) have the ability to alter their shape and characteristics when exposed to light, temperature, electricity, moisture, or other external stimuli [1–4]. SMPs can be transformed into multiple shapes by programming polymer networks. In addition, they can withstand large strains when compared to other materials [4]. Hence, they show potential as materials for applications in sensor technology, micro-actuation, and textile filaments, as indicated by Refs. [5,6]. Amidst the different categories of SMPs, thermoresponsive SMPs are widely used because of their simple operation. Shape-memory polyurethane (SMPU) is a representative thermoresponsive polymer. An essential condition for the shape-memory behavior of an SMPU is its dual-segment structure [7]. The hard segment, which mainly comprises isocyanate groups, serves as a network point that stabilizes the network through physical crosslinking owing to hydrogen bonding and retains the original shape. The soft segment, an ether or ester-based flexible chain, serves as a molecular switch that fixes the temporary shape and enables shape recovery through a phase transition at the transition temperature, e.g., the glass transition temperature (T_g) or melting temperature (T_m). Unlike other SMPs, the soft polyether (or polyester) diol in T_m-type SMPU undergoes polymer crystallization [8–11]. Semicrystalline SMPUs exhibit excellent mobility and immediate shape recovery when exposed to temperatures above T_m.

To design segmented thermoplastic polyurethanes (TPUs), we must understand the molecular behavior of each segment in copolymer systems. Many researchers have studied the effect of the hard-segment content (HSC) on the macroscopic behavior of various SMPUs [12–15]. For example, some experiments were carried out by Lin et al. [12] to clarify how HSC influences the thermal characteristics and

* Corresponding author.
E-mail address: fafala@cau.ac.kr (S. Yang).

https://doi.org/10.1016/j.polymertesting.2024.108531
Received 1 May 2024; Received in revised form 3 July 2024; Accepted 23 July 2024
Available online 24 July 2024

[1]**Abbreviation**

SMPU	Shape-memory polyurethane
DPD	Dissipative particle dynamics
MDI	4,4′-diphenylmethane diisocyanate
PEO	poly(ethylene oxide)
SMP	Shape-memory polymers
TPU	Thermoplastic polyurethane
HSC	Hard segment content
PU	Polyurethane
MD	Molecular dynamics
AA	All-atom
CG	Coarse-grained
COMPASS	Condensed-phase Optimized Molecular Potential for Atomistic Simulation Studies

shape-memory property of TPUs. Also, an examination was carried out by Li et al. [13] to explore the impact of both HSC and the length of the soft segment on the crystallinity and structure of polyurethanes (PUs). Recently, some researchers have focused on computational studies, particularly mesoscale simulations [15–24], to reveal the molecular structures, phase separations, or shape-memory mechanisms of various polymer systems. Mesoscale models treat multiple atoms as a single bead, thus reducing the degrees of freedom and significantly increasing the time and length scales of simulations that are limited to conventional all-atom molecular dynamics (AA MD) models. In our previous study [15], a coarse-grained (CG) MD model was developed to describe the polymer crystallization of long polyurethane chains, which was difficult to implement using AA MD simulations. The developed model made significant advances in providing a crystalline-isotropic thermal transition and observing the molecular behavior of each segment at the nanolevel, such as physical crosslinking of the hard segment or polymer crystallization of the soft segment. Thus, the effect of the HSC of the SMPU copolymer on the thermomechanical properties and shape-memory performance was analyzed.

Another notable aspect is the SMPU structure, consisting of hard and soft segments and causing phase separation [25–27]. Phase separation in SMPUs occurs due to the inherent incompatibility between the two segments, forming distinct domains. The shape memory and mechanical properties of polymeric materials are significantly influenced by their structural completeness and phase separation [28]. Ji et al. studied the shape-memory mechanism of polyurethane in depth and investigated the morphology of the hard-segment domain according to HSC [41,56]. In these studies, the morphology and shape memory performance of various SMPUs were observed using multiple techniques such as DSC, DMA, and SAXS. They revealed that as HSC increases, some Tm-SMPUs show morphological characteristics that change from no hard phase to isolated hard phase and interconnected hard phase. Therefore, to design SMPUs effectively, comprehending the molecular structure of each segment and microphase-separated morphology of the system is crucial. The importance of phase separation analysis can be applied not only to polyurethane itself, but also to shape memory materials composed of polymer blends. Zheng et al. [57] proposed improved shape memory performance compared to conventional polymer blends by using thermoplastic polyurethane (TPU) and polycaprolactone (PCL) to construct a multilayer structure with co-continuous morphology. This architecture is characterized by high morphological continuity of each phase region, and based on phase separation, it significantly improves the dual- or triple-shape memory process by utilizing additional poly(butylene succinate) (PBS) or carbon nanotube (CNT) [58,59]. In addition, analyzing these phase separations in various other materials is also important. Zhang et al. [29] developed a combination of styrene–butadiene–styrene copolymers and poly(ε-caprolactone) blend to explore its shape-memory characteristics. They demonstrated that the phase morphologies of the immiscible blend played a crucial role in achieving shape recovery and fixing. Similarly, in polymer-based materials such as Mater-Bi-type bioplastics [30], the effect of phase separation on their mechanical properties is significant. Various additives have been tested to enhance the miscibility and solubility of gum rosin and its derivatives.

Therefore, understanding and optimizing phase separation is vital for determining the performance of SMPU systems. There are many different types of hard segment diisocyanate, and soft segments also include polyester with carbonyl (C═O) groups and polyether with alkoxy oxygens (-*O*-). Depending on the components of the SMPU, the strength of the hydrogen bonding and crystalline formation vary, which can have a significant impact on the phase separation pattern and domain size. Experimentally, it is very time-consuming to observe the phase-separated morphology of these various design variables one by one and understand the shape-memory mechanism. Therefore, it is necessary to design and predict phase-separated morphology according to target material and molecular weight through simulation.

As shown in Fig. 1, atomistic-scale models, such as AA MD, which consider all atomic degrees of freedom, are unsuitable for studying the phase separation behavior of SMPU copolymers. Therefore, a mesoscale simulation model, which is an intermediate concept between the atomistic and continuum scales, is required to understand the microphase-separated morphology. We developed CG MD models in a previous study [15], which were bead models with 8–13 nm long unit cells, to implement polymer crystallization, a mesoscale phenomenon, and fully described the shape-memory cycle for semicrystalline polymers. However, considering that the size of the polymer microstructure is generally of the order of 10 nm and that a hard-segment domain of tens of nanometers is found in PU with high HSCs [31,32], the CG MD model also has limitations in observing the microphase-separated morphology of SMPUs.

In this study, the dissipative particle dynamics (DPD) method was adopted to focus on the polymer mixing phenomenon rather than the molecular behavior of each polymer chain. To observe the phase separation and phase morphology on a scale of tens of nanometers, using a DPD strategy that can further simplify the simulation model and expand the computational scale is effective. Similar to a previous study [15], we modeled an SMPU copolymer in which a urethane bonding was created by linking hard-segment 4,4′-diphenylmethane diisocyanate (MDI) and soft-segment poly(ethylene oxide) (PEO). Then, each bead was defined to represent each segment. The mesoscale DPD potentials were systematically derived using the solubility parameter of each segment calculated through an AA MD simulation. Finally, the change in the phase morphology of the segmented SMPU was investigated, and complete evolution of the phase architectures was elucidated based on the HSC. Our structural model for SMPU involves all the morphological cases discussed in various studies [18,22,33–41] for polyurethanes and emphasizes the specific features of SMPs. The phase separation analysis using this DPD model can help understand the shape-memory mechanism of semicrystalline SMPU in correlation with the behavior of each segment and shape-memory performance investigated using our previous CG MD model. These two mesoscale models have complementary characteristics; notably, through their integration, a package that can fully understand the mesoscale phenomena and operating mechanisms occurring in smart stimuli-reactive materials has been built.

2. Methods

2.1. Dissipative particle dynamics (DPD) simulation

The DPD simulation proposed by Groot and Warren [42] is a mesoscale technique that enables the study of the dynamic and rheological characteristics of simple and complex fluids. DPD simulations can focus on molecular behavior in mesoscale phenomena, such as polymer–solvent dissolution and phase separation, by simplifying multiple

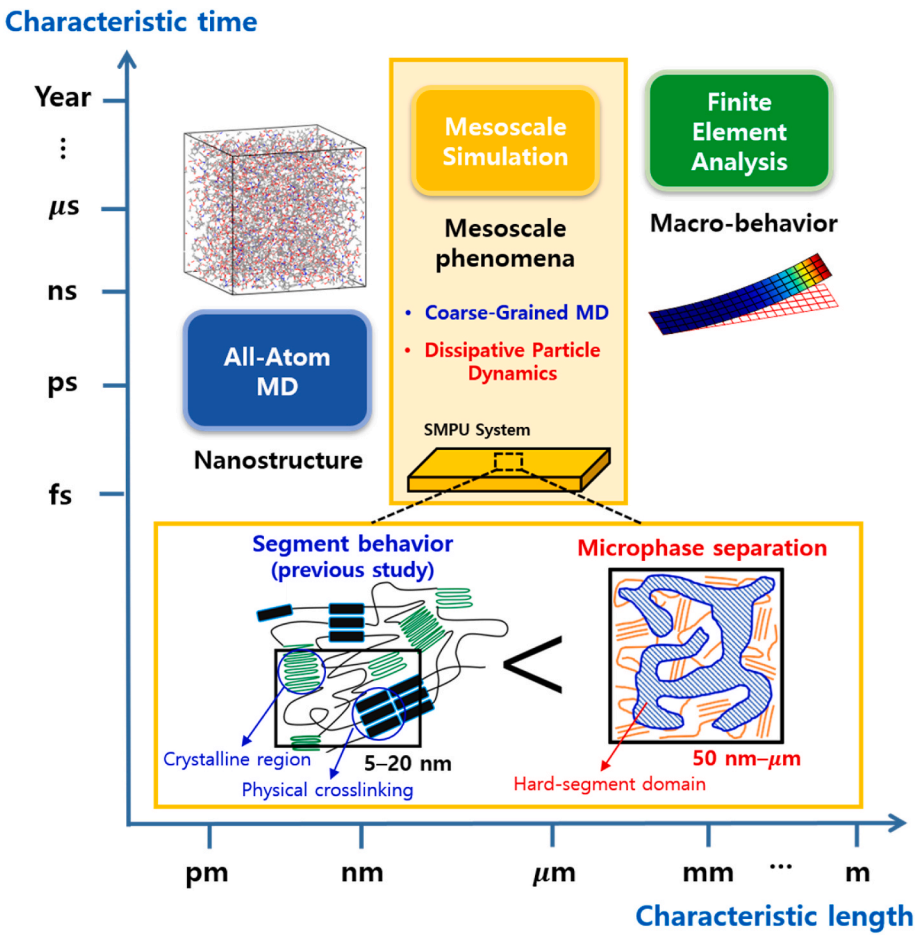

Fig. 1. Mesoscale simulation-based strategy for analyzing phase separation behavior in an SMPU system.

atoms into a single bead. The DPD simulation employs Newton's equation of motion for all beads, where r_i, v_i, m_i, and f_i represent the position, velocity, mass, and force acting on each particle, respectively.

$$\frac{dr_i}{dt} = v_i, m_i\frac{dv_i}{dt} = f_i = \sum_{j\neq i}\left(F_{ij}^C + F_{ij}^D + F_{ij}^R\right) + F_{ij}^S \tag{1}$$

Bead i experiences a combined force (f_i) comprising four components: conservative (F_{ij}^C), dissipative (F_{ij}^D), random (F_{ij}^R), and spring (F_{ij}^S). The conservative force is described by Equation (2) and represents a soft repulsion acting along the line connecting the centers of the beads. It gradually decreases to zero as the distance between the beads reaches a specific cutoff radius (r_c).

$$F_{ij}^C = \begin{cases} a_{ij}\left(1 - \frac{r_{ij}}{r_c}\right)\hat{\mathbf{r}}_{\mathbf{ij}}, (r_{ij} < r_c) \\ 0, (r_{ij} > r_c) \end{cases} \tag{2}$$

Here, the polymer chains have no entanglement because of their relatively simple and weak nonbonding interactions. Therefore, the repulsion of the DPD model focuses more on the mixing phenomenon between different components rather than accurately replicating the structure of the polymer chain itself, as in the CG MD model developed using the previous iterative Boltzmann inversion method [15]. Thus, the DPD simulation significantly extends the time scale and facilitates an in-depth exploration of the polymer phase mixing and separation behavior.

The repulsion parameter (a_{ij}) is considerably significant in characterizing the interactions among DPD beads; therefore, we utilized the theory proposed by Groot and Warren [42] and an all-atom MD simulation scheme to determine accurate values for this parameter in this study. According to that theory, the Flory–Huggins parameter (χ) is used to determine the repulsion parameters between different types of beads. This parameter can be computed based on the difference in solubility (δ) between molecular components. Solubility parameters represent the chemical and physical characteristics of a material and provide insights into the heat of mixing of liquids and amorphous polymers. The dissimilarity in solubility ($\delta_i - \delta_j$) between two substances is employed to evaluate the mixing ability of a binary system without any significant specific interaction, such as noncombinatorial entropy effects or hydrogen bonding. The process of deriving the repulsion parameter is described in detail in Section 2.2.

Equation (3) represents the relationship between the dissipative force (F_{ij}^D) and relative velocity of the particles, indicating that as the relative velocity increases, the dissipative force also increases, reducing their momentum. By contrast, the random force (F_{ij}^R) serves as a compensatory force, offsetting the energy loss caused by the dissipative force.

$$F_{ij}^D = -\gamma\omega^D(r_{ij})(\hat{\mathbf{r}}_{\mathbf{ij}} \bullet \mathbf{v}_{\mathbf{ij}})\hat{\mathbf{r}}_{\mathbf{ij}}, F_{ij}^R = \sigma\omega^R(r_{ij})\frac{\xi_{ij}}{\sqrt{\Delta t}}\hat{\mathbf{r}}_{\mathbf{ij}} \tag{3}$$

The frictional and random forces are characterized by the weight functions $\omega^D(r_{ij})$ and $\omega^R(r_{ij})$, along with the amplitude coefficients γ and σ. According to Español and Warren's theory [43], these weight functions are mutually dependent and related to the Boltzmann constant and system temperature, as shown in Equation (4). ξ_{ij} represents a random number with a mean of 0 and variance of 1, independent of all the pairs of interacting particles at every time step. Groot et al. [42] proposed

simplifying the weight functions, where $\omega^R(r_{ij})$ has the same form as the conservative force, as shown in Equation (5).

$$\omega^D(r_{ij}) = \left[\omega^R(r_{ij})\right]^2, \sigma = \sqrt{2\gamma k_B T} \tag{4}$$

$$\omega^D(r_{ij}) = \left[\omega^R(r_{ij})\right]^2 = \begin{cases} \left(1 - \frac{r_{ij}}{r_c}\right)\hat{r}_{ij}, (r_{ij} < r_c) \\ 0, (r_{ij} > r_c) \end{cases} \tag{5}$$

The last force term is the spring force (F_{ij}^S), which corresponds to the bonded harmonic potential energy (U_i^S) and can be represented by Equation (6). In this research, the spring constant value (C_b) was set to 4, and the equilibrium bond length ($r_{b,0}$) was set to 0.1 Å for the interconnected beads in the SMPU polymer chains.

$$U_i^S = \sum_b \frac{1}{2} C_b (r_b - r_{b,0})^2, F_{ij}^S = -\frac{\partial U_i^S}{\partial \boldsymbol{r_{ij}}} \tag{6}$$

The bonded potential also shows the simplicity of the DPD model compared to that of the previous CG model [15], which used a multi-center Gaussian distribution to simulate the structural characteristics of the SMPU chain accurately. The dissipative particle dynamics method used in this study is a very suitable method for analyzing the phase separation form of polymers and has endless applications. Based on polymer materials, it is used in various fields such as phase separation of immiscible mixtures [65], filler and matrix relationships in polyurethane composites [66], polymer-gold atom interaction [67], and polymer-solvent interaction [63].

2.2. DPD bead mapping and repulsion parameter derivation

First, a DPD bead was defined for the SMPU system used in the simulation. The thermoplastic SMPU copolymer comprises MDI (hard segment) and PEO (soft segment). To observe the phase morphology by the phase separation of the two segments, one bead was defined for each segment. Unlike the previous CG model [15], which splits the anisotropic MDI into two bead types to extract accurate RDF peaks in the DPD model, the MDI unit was treated as one bead. According to the Flory–Huggins theory [44], ensuring that all beads in the DPD simulations have comparable volumes is necessary. As shown in Fig. 2a and Table 1, the monomer volume in each segment was obtained using the atomistic van der Waals surface provided by the Material Studio 2016 package (BIOVIA, Inc.). Therefore, one MDI (bead M) and five ethylene oxide monomers (bead P) are mapped with DPD beads for each segment to have the same volume (about 250 Å^3).

Next, the repulsion parameter between the DPD beads in Equation (2) was defined. The repulsion parameter, which is the most important factor in the phase separation simulation, can be derived from the Flory–Huggins parameter, which can be calculated from the difference in solubility of each segment. All-atom MD simulations were performed using Material Studio 2016 to obtain the relevant factors.

As shown in Fig. 2b, we constructed amorphous unit cells containing the components corresponding to each DPD bead. The information on each unit cell is provided in Table 2. For each unit cell, geometry optimization (conjugate gradient), followed by 1 ns of the NPT ensemble (at 300 K and 0.1 MPa) and another 1 ns of the NVT ensemble (at 300 K), were performed sequentially. In this study, an ab initio Condensed-phase Optimized Molecular Potential for Atomistic Simulation Studies (COMPASS) force field [45] was used for both the intra and intermolecular interactions. The van der Waals interactions and Coulombic forces were calculated using the Ewald method with a cutoff distance of 12.5 Å. During the MD runs, the temperature and pressure were controlled using an Andersen thermostat [46] and Berendsen barostat [47], respectively. The time step for the dynamic simulations was set to 1.0 fs.

Through the last 100 ps NVT ensemble frames, we calculated the cohesive energy (E_{coh}) of each unit cell to apply the solubility theory. Equation (7) outlines the process of acquiring the energy values for each molecule ($E_{isolated,i}$, i = 1-$N_{molecule}$) and the overall bulk system (E_{bulk}) by performing a single-point energy calculation with the fully equilibrated MD unit cell.

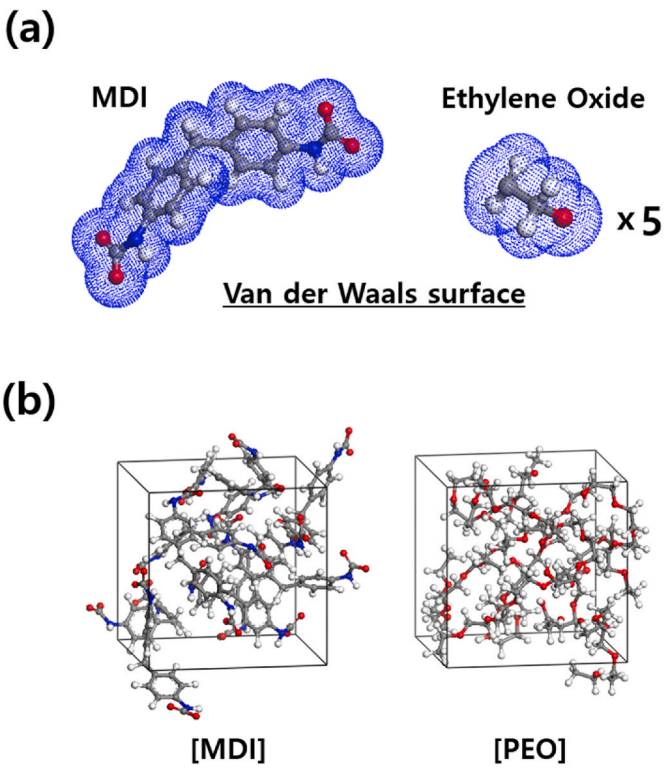

Fig. 2. (a) Monomer volume calculation of each segment through van der Waals surface (b) All-atom MD configurations of pure MDI and PEO unit cells. Detailed information is listed in Table 2.

Table 1
DPD bead mapping with similar molecular volume for each segment of the SMPU.

	$V_{monomer}$ [Å^3]	No. of monomers per DPD bead	DPD V_{bead} [Å^3]
MDI (Hard segment)	243.65	1	243.65
PEO (Soft segment)	51.03	5	255.15

Table 2
Information on the all-atom MD unit cells of the constituents of each DPD bead.

Unit cell	No. of constituents	Density (g/cm^3)
MDI	10 MDI monomer (10 M beads)	1.29
PEO	10 ethylene oxide (EO) pentamers (10 P beads)	1.06

$$E_{coh} = \frac{\left(\sum_{i=1}^{N_{molecule}} E_{isolated,i}\right) - E_{bulk}}{N_{molecule}} \tag{7}$$

$$\delta = \sqrt{E_{coh}/V} \tag{8}$$

$$\chi_{ij} = \frac{V_{bead}}{k_B T}(\delta_i - \delta_j)^2 \tag{9}$$

$$a_{ij} = a_{ii} + \frac{\chi_{ij}}{0.286} \ (a_{ii} = 25, \rho = 3) \quad (10)$$

The solubility parameter (δ in Equation (8)) and χ-parameter (Equation (9)) were consecutively computed based on the derived cohesive energy (E_{coh}). The calculation involved several variables such as the molar volume of the MD unit cell (V), volume of the DPD bead (V_{bead}) equals to 252 Å^3, Boltzmann constant (k_B), and temperature (T). Finally, the χ-parameter was used to determine the repulsion between two different types of beads. Groot et al. [42] introduced Equation (10) while considering the dimensionless bead density (ρ = 3). To ensure the equivalent compressibility of water, the repulsion parameter for identical beads was set to $a_{ii} = 25$ [42]. In this SMPU system, the self-interaction parameter (a_{ii}) for bead M was assigned a value of 22.5 instead of the usual value of 25. This specific value was chosen to accurately depict the hydrogen bonding that occurred between the MDIs and was also applied in previous studies [48,49]. Hence, in the DPD simulation, the magnitude of the repulsive parameter between different beads is much larger or smaller than these a_{ii} is important for the mixing behavior of dissimilar materials. The calculated solubility parameters for each segment and the resulting repulsion parameters are shown in Tables 3 and 4, respectively. Notably, the solubility parameters show remarkable agreement between the calculated results (MDI: 28.71 $(J/cm^3)^{1/2}$; PEO: 23.14 $(J/cm^3)^{1/2}$) and other experimental and computational results [18,50–52] (MDI: 27.15–28.5 $(J/cm^3)^{1/2}$; PEO: 20.2–24.5 $(J/cm^3)^{1/2}$) as shown in Table 3. This meticulous approach to determining the repulsion parameter significantly enhanced the dependability of the resulting DPD study.

2.3. DPD unit cell Construction and simulation conditions

As shown in Fig. 3a, we constructed SMPU chains for the DPD simulations with five different HSC values (15, 21, 32, 45, and 50 wt%). The molecular weights of the polymer chains are 3.33–5.72 × 10^5 g/mol, which is 10 times that of previous CG models [15] and corresponds to or exceeds the experimental molecular weights of thermoplastic polyurethane [33,53]. When the soft segment (PEO) length is fixed, the HSC is increased by increasing the hard segment (MDI) length. Information on each chain is shown in Table 5.

Moreover, to perform a DPD simulation, establishing reduced units for mass, length, energy, and time is essential. The mass unit corresponds to the mass of the DPD beads, while the length unit is defined as the size at which the dimensionless bead density of a unit-length cube reaches 3 (ρ = 3). The energy was set to $k_BT = 1$. By utilizing these predefined units, the timescale unit is calculated within a reduced unit system. Table 6 shows the formula for obtaining the reduced units and specific values employed in this study. The mass scale in the DPD simulation was determined by considering the average mass of the beads based on the HSC (15–50 wt%) of the SMPU, and corresponding time scale value was determined accordingly. In Table 6, all the reduced unit values at each scale are defined as 1, representing the unit scale in the DPD simulation.

Next, we constructed DPD unit cells having a size of $30L \times 30L \times 30L$ ($27.3\,nm \times 27.3\,nm \times 27.3\,nm$) using the reduced units. The simulation time step was defined as τ = 0.05t, energy scale (temperature) was set to 1, cutoff distance was 1 ($r_c = 1$), and total simulation time was set to 2 × 10^5 τ. Each unit cell comprised ~8 × 10^4 DPD beads with a dimensionless bead density of 3 (ρ = 3).

Table 3
Solubility parameter (δ) of MDI and PEO obtained from all-atom MD simulations.

Solubility parameter δ ($\sqrt{J/cm^3}$)			
MDI		PEO	
Cal.	Ref. [18,50]	Cal.	Ref. [51,52]
28.71	27.15–28.5	23.14	20.2–24.5

Table 4
Final repulsion parameters (a_{ij}) for DPD simulations.

bead type[a]	M	P
M	22.5[b]	
P	31.59[c]	25[c]

[a] Bead type (M: MDI; P: PEO).
[b] Urethane hydrogen bonding (Ref. [48,49]).
[c] Solubility theory (Groot et al. [42]).

While a larger simulation box would be ideal for minimizing finite size effects, its implementation was deemed too time-consuming. Therefore, the unit cell size and total simulation time used in this simulation were set above sufficient values to reach the equilibrium state used in several DPD studies [60–63]. Moreover, it was discovered that the size of the simulation box has no impact on the radius of the phase domain [64]. Therefore, the size of the unit cell and other simulation conditions used in this DPD simulation were appropriately adopted.

3. Results and discussion

3.1. Phase separation of segmented thermoplastic SMPU

Fig. 4 illustrates the changes in phase morphology according to the time step in the DPD simulation of the PU 15 model. The unit cell contains two different beads: the yellow beads represent M (MDI) beads, and the green beads represent P (PEO) beads. After the initial state, the PEO beads were hidden to visualize the morphology of the hard domains better. The M beads, initially dispersed within the MDI–PEO mixed phase gradually aggregated and formed a phase morphology that approached a state of equilibrium at approximately t = 100,000τ. In the final configuration, the hard phase formed several isolated particulate domains, and the phase structure of MDI was completely distinct from the soft-segment PEO phase. The phase-separated SMPU observed in the DPD simulation comprehensively captured the influence of the hydrogen bonding of MDI ($a_{ii} = 22.5$) and incompatibility between the hard and soft segments ($a_{ij} = 31.59$).

To illustrate the phase domain connections and distributions more effectively, we observed the phase morphologies of 2 × 2 × 2 cells under periodic boundary conditions. Fig. 5 shows the morphology of the hard-segment phase according to the HSC ((a) 15, (b) 21, and (c) 32 wt%) and provides some views from specific directions of the simulation box. As shown in Figs. 4 and 5a, the MDI phase of SMPU containing 15 wt% of HSC takes the form of spherical domains. They formed distinct and separate domains within the soft-phase region, with no interconnections between the individual domain areas. Although SMPU is a copolymer structure composed of hard and soft segments, the observed structural arrangement resembles that of a nanofiller embedded in a polymer matrix. These findings align with the experimental results [33–35] that demonstrate the presence of isolated spherical hard-segment domains in polyurethane with a low HSC, thereby confirming the validity of our DPD model.

The HSC 21 wt% model (Fig. 5b) exhibited the formation of similar phase domains, along with the additional formation of worm- or rod-shaped domains [36,37], which are slightly larger hard clusters. Even in the PU 21 model, the hard-segment domains still had isolated areas that were not connected to each other. For PU 32 (Fig. 5c), a stronger connection was established between the MDI beads in a specific direction. Consequently, the hard segment within a single unit cell existed as several "short cylinders" [37–39]. These cylindrical shapes formed an alternating structure of hard and soft segments in a 2 × 2 × 2 periodic unit cell, creating a "lamellar" microdomain structure. The thickness of the lamellae and space between them can be modified by changing the molecular composition or chain length of SMPU [35,39,40]. This

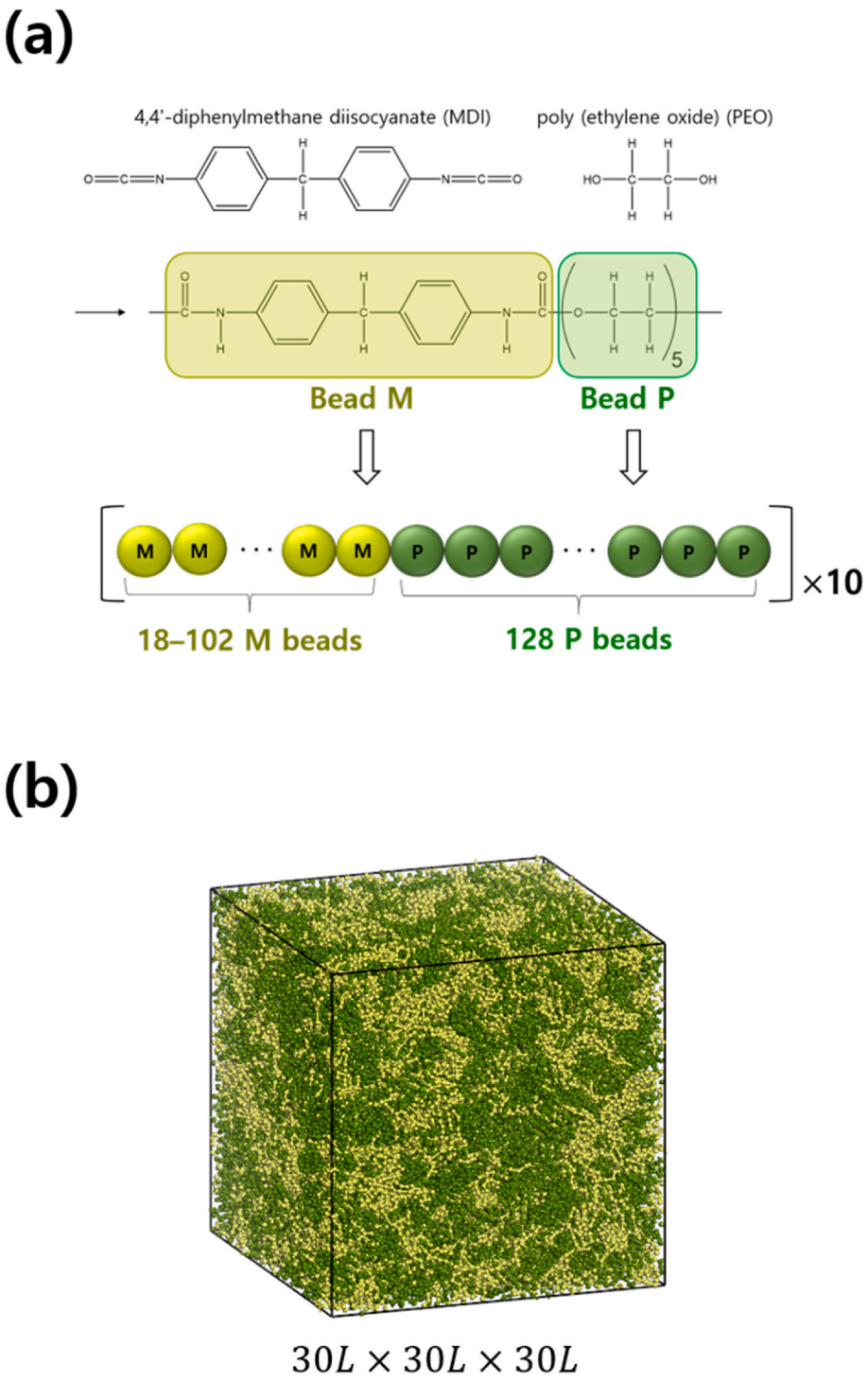

Fig. 3. (a) Design of SMPU chains for DPD simulation (b) Unit cell of DPD simulation with a length of 30 as a reduced unit.

Table 5
Information on the DPD chains with 5 different HSCs. All the models consist of an equal quantity of soft-segment (P) beads, i.e., 1280 beads.

Model	HSC [wt. %]	No. of hard-segment (M) beads	Molecular weight [kg/mol]
PU 15	15.27	180	333.1
PU 21	21.28	270	358.7
PU 32	32.46	480	418.4
PU 45	45.68	840	520.7
PU 50	50.52	1020	571.9

Table 6
Information on the reduced units in DPD simulation.

DPD unit	Equation	Reduced unit
Length scale	$L = (V_{bead} * 3)^{\frac{1}{3}}$	9.1112 Å
Mass scale	$M = M_{bead}^{avg}$	230–264 amu
Energy scale	$E = k_B T$ (300 K)	0.59616 kcal/mol
Time scale	$t = L\sqrt{M/E}$	8.75–9.37 ps

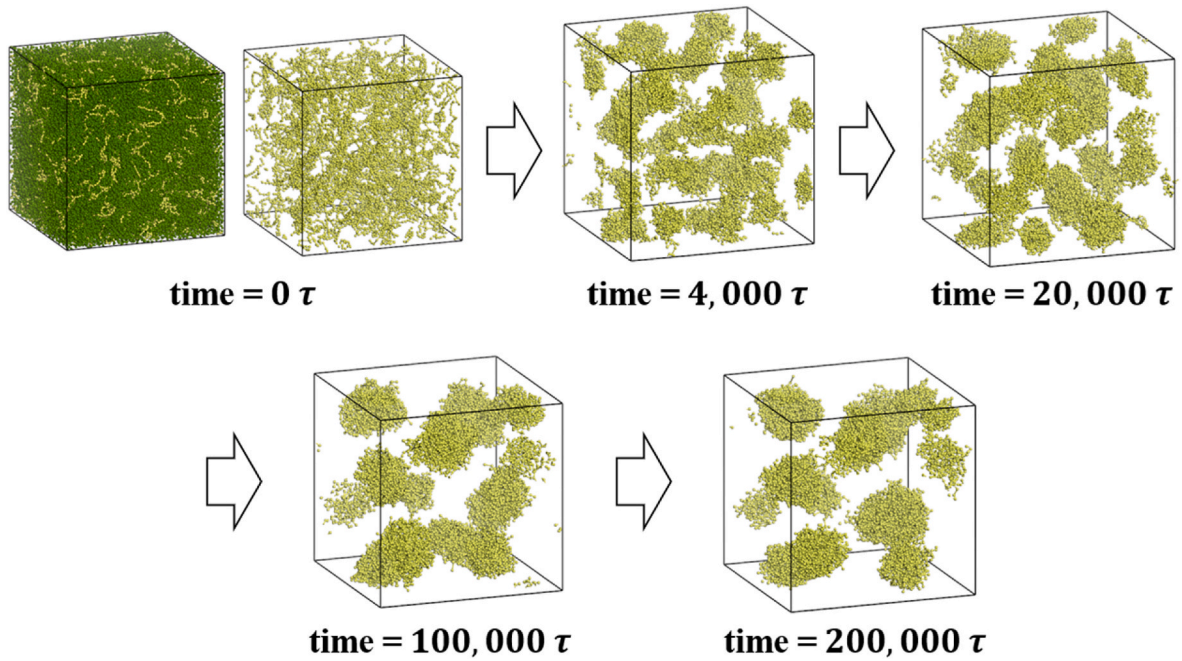

Fig. 4. Structural evolution of the phase domain of the PU 15 model by phase separation according to the time step of DPD simulation. Yellow beads represent MDI, and green beads represent PEO. To illustrate the hard-segment domain more effectively, PEO beads are hidden from view. (For interpretation of the references to colour in this figure legend, the reader is referred to the Web version of this article.)

microdomain structure plays a significant role in influencing the thermomechanical properties of segmented polyurethane copolymers.

Fig. 6 shows the probability density for the number of beads M (MDI) constituting a single cluster of hard segments in the unit cell of each model. As the HSC increased, the hard segment domains gradually changed from clusters with 252–1530 MDI beads to clusters with 999–4618 MDI beads, followed by short cylinders or lamellar structures. Therefore, the initially isolated regions with sizes of 4–11 nm (HSC = 15 wt%) and 7–21 nm (HSC = 21 wt%) were further connected to each other to develop into a lamellar structure (HSC = 32 wt%), forming a wave in a specific direction. Here, we observe that hard-segment lamellae with a thickness of ~10–15 nm were repeated with an interdomain space of ~20 nm. Several experimental studies [38,54,55] showed that alternating hard and soft stripes or lamellar structures appear in models with HSCs >~30 wt%, and the interdomain spacings were ~10–20 nm. These results support the validity of our DPD results, which correspond to observations at a scale of ~55 nm (2 × 2 × 2 unit cell).

The properties of MDI-based SMPs primarily depend on the MDI, which maintains a permanent shape. According to previous studies [18,22], when the HSC of the SMPU block copolymers increases, the hard segments agglomerate to form stable domains. Fig. 7 shows the phase morphologies of the PU 45 and PU 50 models with further increases in the HSC, as shown in Fig. 5. Stronger interconnections between the hard domains were observed in PU 45 (Fig. 7a) than in PU 32. Therefore, the phase morphology, which was in the form of a stripe, developed into an "interconnected" phase throughout the entire unit cell. In addition, in PU 50 (Fig. 7b), the hard domain formed a "continuous" region that governed the entire system of the SMPU.

3.2. Architectural evolution of phase morphologies

The structure of the MDI phase represents a network with the netpoint of SMPU models, which progressively becomes stronger as the HSC increases. Within a specific range of HSC, the hard-segment phase undergoes a transformation from a spherical domain to a continuous domain. Fig. 8 summarizes the architectural evolution of the hard domain (MDI) based on the molecular composition of SMPU, illustrating the resulting morphology characterized by phase separation between the hard and soft segments. We propose that the phase architectural evolution of a unit cell, as depicted in Fig. 8, accurately represents the SMPU model with varying HSC. As the HSC increases from 15 to 50 wt%, the isolated spherical structure of the MDI phase transforms into a rodlike structure, followed by cylindrical/lamellar formations, and finally, an interconnected/continuous structure. The mesoscale outcomes obtained through the DPD simulation align with the experimental findings [38,41], which indicate that the hard segment of thermoplastic polyurethane progresses from an isolated spherical state to a rodlike structure, followed by cylindrical/lamellar and finally an interconnected/continuous structure. Therefore, the hard segment of an SMPU gradually builds a rigid framework as the HSC increases, whereas the soft segment changes from the filling matrix phase to the minor remaining phase. The phase morphologies of each segment obtained by phase separation can be further used to discuss the shape-memory behaviors of the SMPU system.

3.3. Mechanism of shape-memory properties

Based on these mesoscale studies, the shape-memory mechanism of semicrystalline SMPUs is summarized in the MDI/PEO system. These particular SMPs necessitate a combination of two components that do not mix. The first component is isocyanate, which establishes physical crosslinking through hydrogen bonds. The second component is a molecular switch such as a crystalline polyether or ester. The different chemical components of a block copolymer play distinct roles in the shape-memory effect. The MDI phase acts as the network point, whereas the PEO phase serves as the switch. Depending on the HSC, components can exhibit various phase architectures.

In our previous computational work [15], we performed a thermo-mechanical shape-memory cycle of a crystalline SMPU. We simulated a mesoscopic shape-memory cycle using CG models in LAMMPS, comprising four steps: loading, cooling, unloading, and reheating. The first characteristic is the shape-fixity ratio (R_f), which describes how well the SMP can fix the temporarily deformed shape after

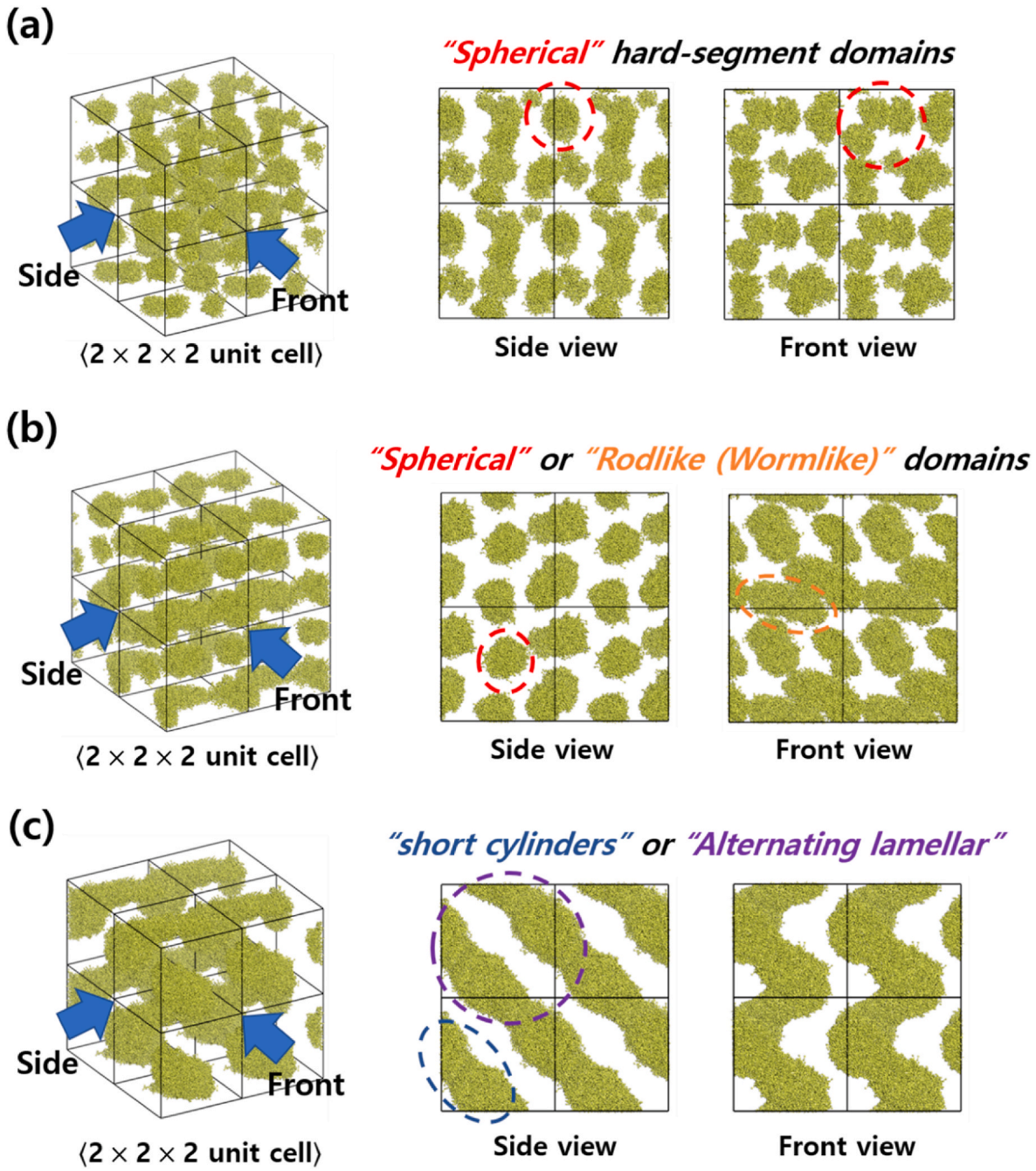

Fig. 5. Phase-separated morphology of hard-segment domains in (a) PU 15 (HSC = 15 wt%), (b) PU 21 (HSC = 21 wt%), and (c) PU 32 (HSC = 32 wt%).

it is cooled and the external stress is removed. The second characteristic is the shape-recovery ratio (R_r), which quantifies the extent of SMP recovery relative to its original shape, in response to being reheated. The detailed simulation conditions and shape memory performance derivation process of the CG model are explained in detail in reference [15].

As a result, as shown in Fig. 9a, the crystallinity and shape memory performance of semi-crystalline SMPU were found to decrease as HSC increased. SMPUs with lower HSCs showed enhanced shape fixity with the high crystallinity of soft PEO. In addition, SMPUs with higher HSCs exhibited poor shape-recovery ability owing to the degraded mobility of the hard-segment chains. To further understand the macroscopic shape-memory behavior of dual-segment SMPU systems, understanding the segment behaviors of the polymer chains and microphase-separated morphology on the scale of tens of nanometers or more is necessary.

According to the DPD results, the concept of shape-memory can be classified into three groups, each presenting a distinct phase structure, as shown in Fig. 9b. Because of their immiscibility, phase separation occurred consistently in the copolymer system. Region I exhibited good shape retention and shape-recovery performances of 95 % or better. This is because both PU 15 and PU 21 have an MDI domain in the droplet (isolated) phase and a PEO domain in the filling matrix phase. The strong crystallization of PEO in the matrix phase provides effective resistance to shape deformation, resulting in good shape-fixing ability. During the reheating process, the crystalline phase was entirely melted, and the hard-segment domain of the isolated phase was completely relaxed; thus, the shape-recovery ability was also good.

Region II was not significantly different from region I in shape-memory performance, and the shape-fixity and shape-recovery ratios were slightly decreased by the different phase morphologies. The MDI domains gradually connected to each other and began to change from an

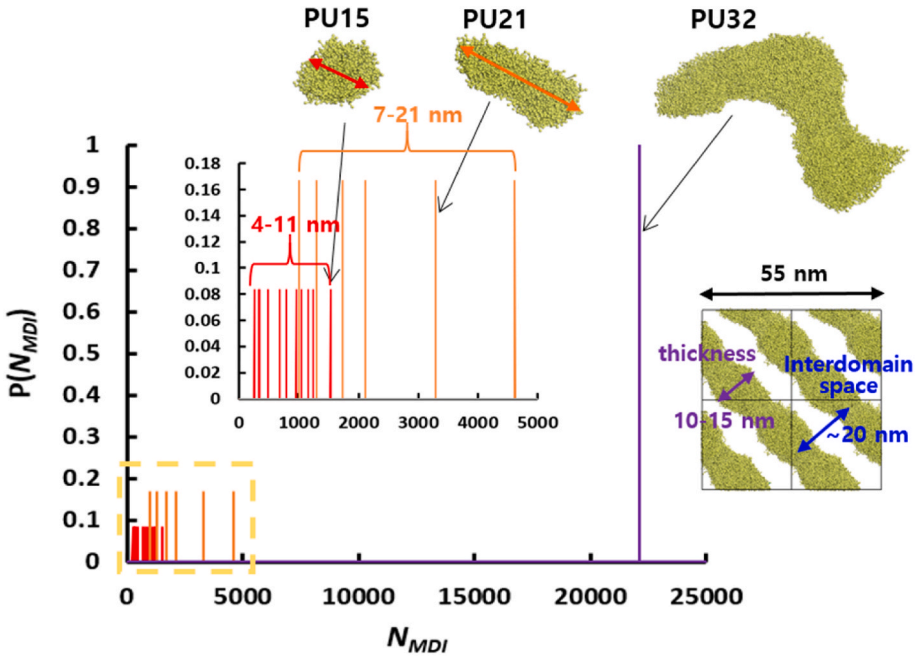

Fig. 6. Probability density for the number of beads M forming each hard-domain cluster in a unit cell of PU 15, PU 21, and PU 32.

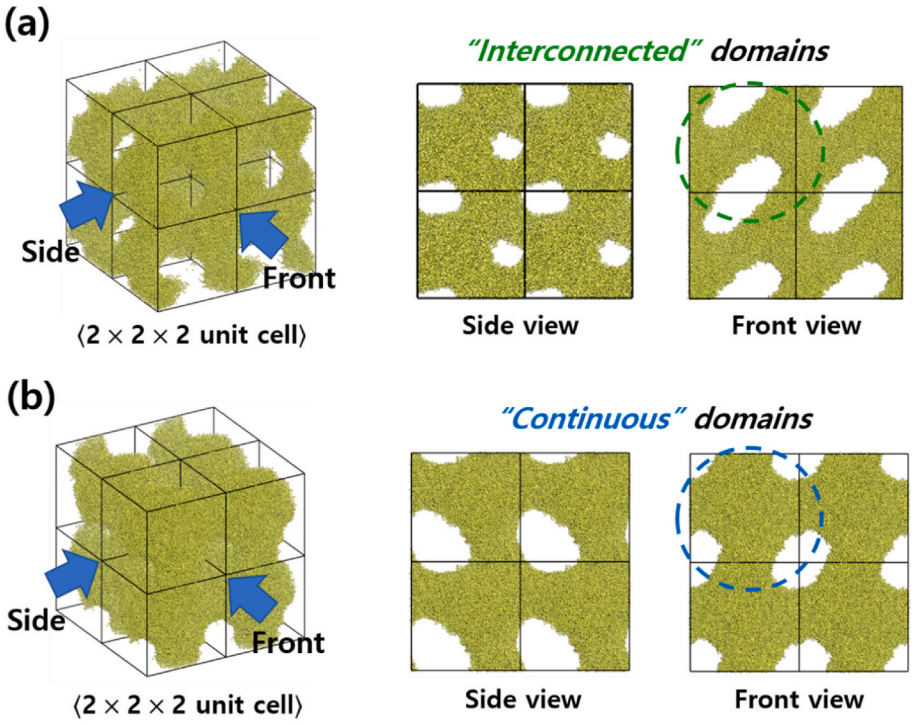

Fig. 7. Phase-separated morphology of hard-segment domains in (a) PU 45 (HSC = 45 wt%) and (b) PU 50 (HSC = 50 wt%).

isolated state to a lamellar (PU 32) or interconnected (PU 45) structure. The strong adhesion between the MDIs reduced the crystallization of the PEO matrix, resulting in a decrease in the shape-fixing ability. In addition, the mobility of the polymer chains in the extended MDI domain was reduced; thus, the recovery performance was also affected.

In Region III, where the HSC was >50 wt%, the hard domain formed a continuous phase and dominated the entire SMPU system. In this region, as the HSC increased, PEO gradually became a minor phase that occupied the remaining space; thus, the crystallinity and shape-fixing ability further deteriorated. In addition, at high HSCs, the rigid framework of the hard phase must be forcibly deformed during the loading process. Therefore, the elastic property of returning to the original shape of the continuous hard-segment domain also caused a rapid decrease in the shape-fixing ability. A reduction in the shape-recovery ratio also caused by the larger deformation of the hard segment domains when transitioning from the isolated to continuous state. When it changed from an isolated to a continuous state, the continuous MDI domain did not completely recover when PEO melted, even at high temperatures.

The optimized design for shape-memory performance involves a

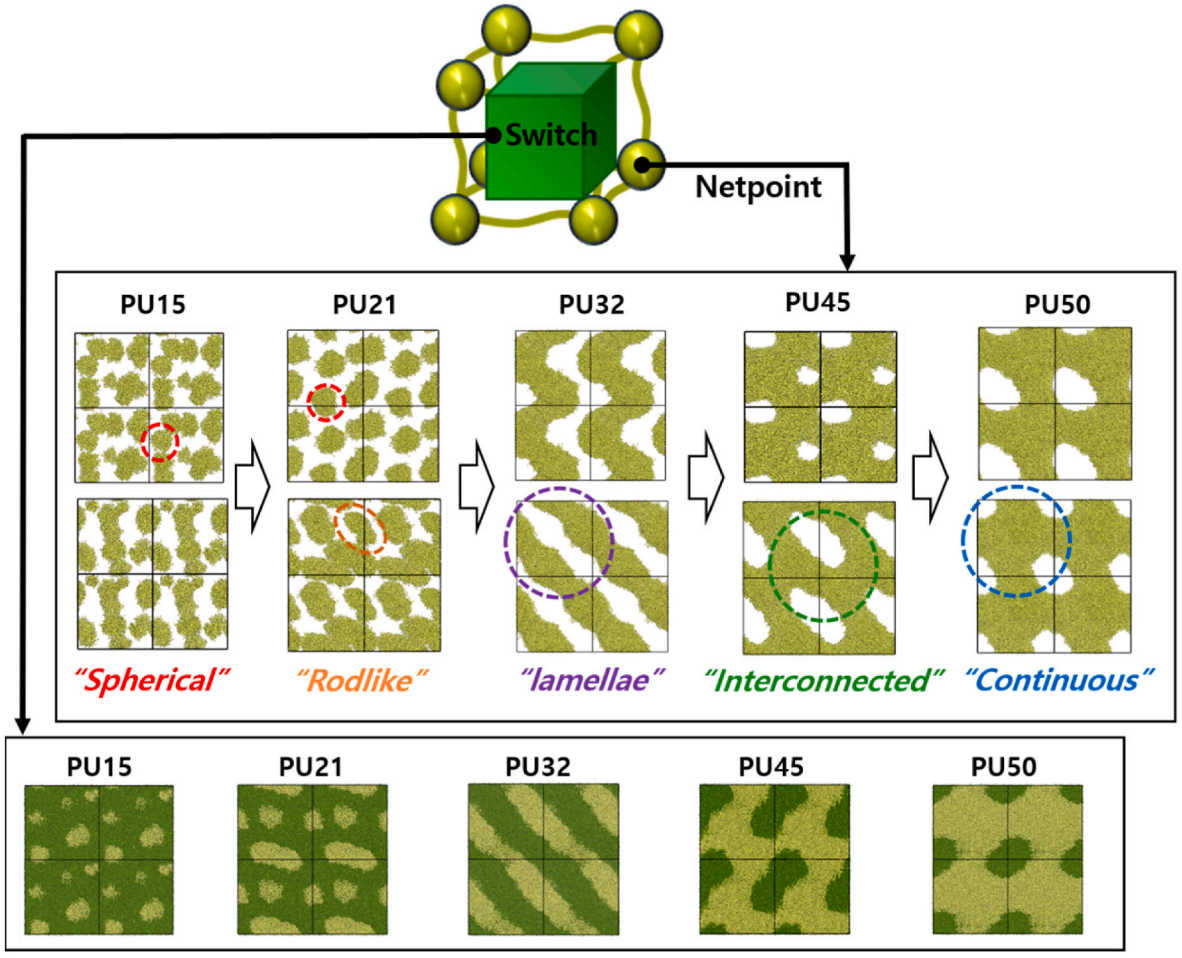

Fig. 8. Illustration for architectural evolution of phase morphologies of hard and soft segments according to HSC (15–50 wt%) of the SMPU.

model in region I where the soft segment acted as the primary matrix phase and hard segment existed as an isolated phase. In this design, the crystalline polymer exhibited excellent fixing and unfixing performances, whereas the hard domain had minimal impact on the recovery performance. The changes in phase domain morphology observed through the DPD model further support previous findings [15,68] that the mean square displacement (MSD), which represents the mobility of SMPU chains, decreases with increasing HSC. Our structural shape-memory model, shown in Fig. 8, encompasses the complete development of the structural phases of the two components of the SMPU. It incorporates every single morphological structure discussed in the literature [18,22,31–39] to validate the reliability of the DPD models and emphasize the distinctive traits of SMPs. By carefully designing the phase shape of immiscible components along with other thermo-mechanical properties (i.e., elastic modulus and melting temperature), it is possible to establish an optimal SMP system characterized by exceptional stability and performance. In addition, if more chain composition ratios, temperature effects, as well as DPD parameters are considered, a more in-depth analysis of phase interface diffusion, such as rotational or translational diffusion of segmented SMP, will be possible [69,70].

4. Conclusion

In this study, a DPD model based on mesoscale simulations was developed to investigate the phase separation morphology and obtain a deeper understanding of the shape-memory mechanism of TPU co-polymers. Our previous CG MD model developed via the iterative Boltzmann inversion method reproduced the crystalline phases and aggregation of hard domains, but the scale was not adequately large to observe the microphase-separated morphology at tens of nanometers or more. To overcome these limitations, the scale of the simulation unit cell was further expanded, and the phase separation rather than the structure of the polymer chain itself was focused on.

In this DPD model, the repulsion parameters between the beads, which indicates the degree of incompatibility, were derived using the solubility theory proposed by Groot et al. The difference in the solubility of each segment calculated through AA MD simulation was applied to the Flory–Huggins theory to determine the final repulsion parameter. This approach significantly improved the reliability of the DPD model. The mesoscale DPD model successfully predicted the phase separation and final morphology of thermoplastic polyurethane at 300 K according to the HSC. The hard-segment phase existed in an isolated or discontinuous state in the low-HSC model (PU 15 and PU 21). At this time, the hard segment exists in the form of droplets in the soft segment and the soft segment acts as a matrix. As the HSC gradually increased, stronger connections were formed between the hard segments, showing a lamellar structure in PU 32 and an interconnected phase in PU 45. In PU 50, a continuous phase was formed in which the hard segment dominated the entire system.

Here, we provide a more in-depth analysis of the shape memory performance of segmented polyurethane from a phase-separated morphology perspective. SMPUs with lower HSC demonstrated superior shape fixity because the crystalline PEO phase functions as a filling matrix, creating spherical MDI domains, thereby enhancing the shape fixity. Conversely, higher HSC resulted in the formation of linked continuous phases between PEO and MDI, leading to diminished shape

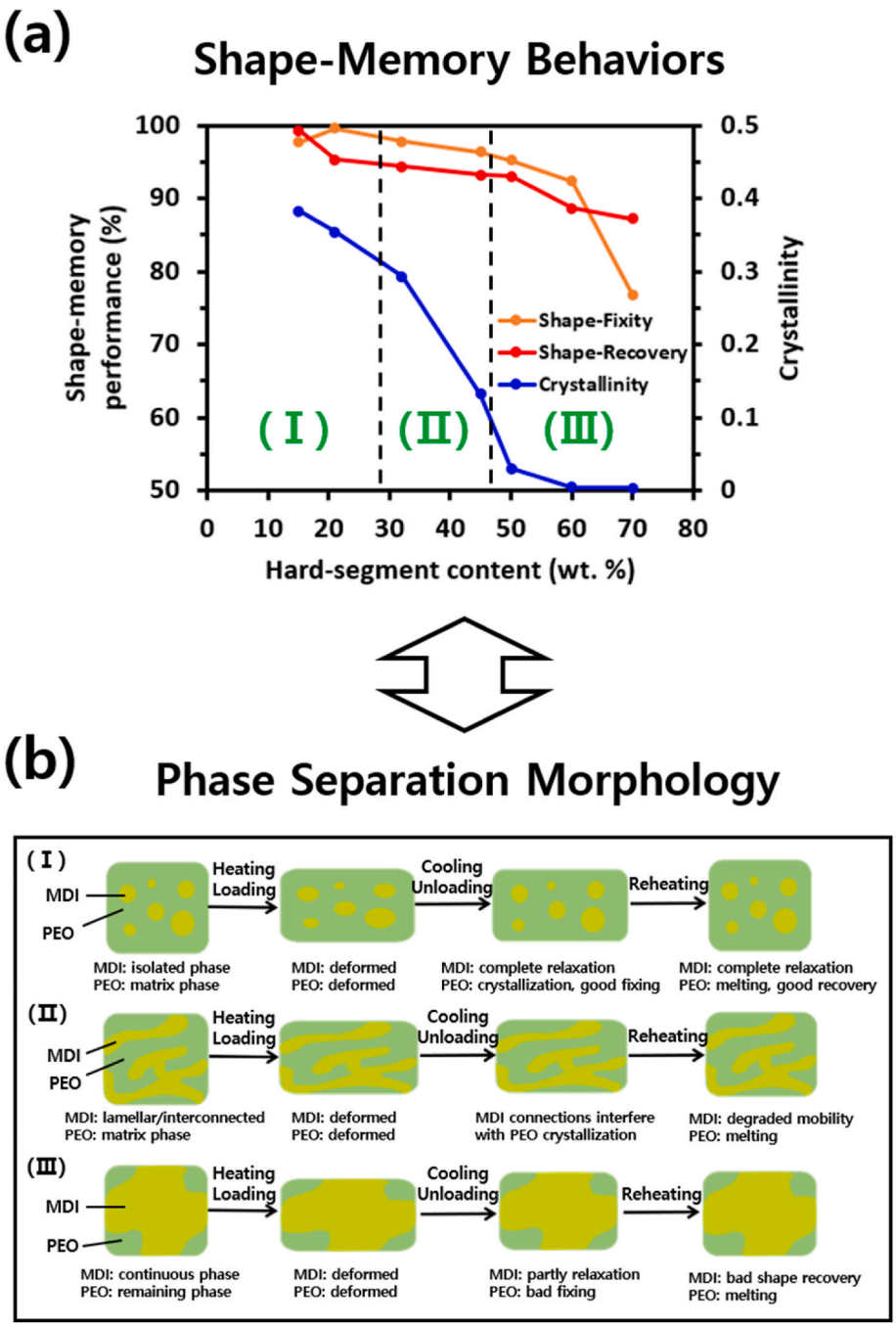

Fig. 9. (a) Shape-memory performances and crystallinity of SMPUs composed of MDI and PEO according to the HSCs (15–70 wt%) [15]. (b) Schematic illustrations of the shape-memory mechanism considering phase separation of thermoplastic MDI–PEO SMPUs.

fixity. The decrease in the shape-recovery ability is owing to the transformation of the hard segment phase from a spherical to a continuous domain. This implies that it is difficult for the rigid hard-domain network, which is forcibly deformed to return to its original shape. Regarding shape-memory performance, the optimized design entails a soft segment serving as the primary matrix phase, whereas the hard segment remains isolated. This design ensures excellent fixing and unfixing capabilities of the crystalline polymer while minimizing the reduction in recovery performance caused by the hard domain.

Our shape-memory structural model is essential for understanding mesoscale phenomena such as phase separation in SMPUs, and it correlates with the shape-memory performance to elucidate the mechanism of the polymer system. It encompasses the complete evolution of the phase architectures of the two components in the SMPU and incorporates various morphological models from the literature. This integration validates the rationality of the DPD models and highlights the distinctive characteristics of SMPs. We expect that the proposed DPD model will be effectively utilized in the structural design of polymers for various functional purposes.

CRediT authorship contribution statement

Sungwoo Park: Writing – original draft, Methodology, Investigation. **Jeong-ha Lee:** Methodology, Conceptualization. **Maenghyo Cho:** Resources, Funding acquisition, Conceptualization. **Yun Seog Lee:** Investigation. **Hayoung Chung:** Investigation, Funding acquisition.

Seunghwa Yang: Writing – review & editing, Supervision, Resources, Funding acquisition, Conceptualization.

Declaration of competing interest

The authors declare that they have no known competing financial interests or personal relationships that could have appeared to influence the work reported in this paper.

Data availability

Data will be made available on request.

Acknowledgement

This work was supported by the Nano & Material Technology Development Program through the National Research Foundation of Korea (NRF) funded by Ministry of Science and ICT(RS-2024-00408845) and the KOREA HYDRO & NUCLEAR POWER CO., LTD (No. 23-Tech-04).

References

[1] J.S. Leng, X. Lan, Y.J. Liu, S.Y. Du, Shape-memory polymers and their composites: stimulus methods and applications, Prog. Mater. Sci. 56 (7) (2011) 1077–1135.
[2] J.L. Hu, Y. Zhu, H.H. Huang, J. Lu, Recent advances in shape-memory polymers: structure, mechanism, functionality, modeling and applications, Prog. Polym. Sci. 37 (12) (2012) 1720–1763.
[3] Q.J. Song, H.M. Chen, S.B. Zhou, K.Q. Zhao, B.Q. Wang, P. Hu, Thermo- and pH-sensitive shape memory polyurethane containing carboxyl groups, Polym. Chem. 7 (9) (2016) 1739–1746.
[4] F.H. Zhang, Z.C. Zhang, Y.J. Liu, H.B. Lu, J.S. Leng, The quintuple-shape memory effect in electrospun nanofiber membranes, Smart Mater. Struct. 22 (8) (2013).
[5] A. Lendlein, R. Langer, Biodegradable, elastic shape-memory polymers for potential biomedical applications, Science 296 (5573) (2002) 1673–1676.
[6] D.J. Maitland, M.F. Metzger, D. Schumann, A. Lee, T.S. Wilson, Photothermal properties of shape memory polymer micro-actuators for treating stroke, Laser Surg. Med. 30 (1) (2002) 1–11.
[7] H. Meng, G.Q. Li, A review of stimuli-responsive shape memory polymer composites, Polymer 54 (9) (2013) 2199–2221.
[8] F.K. Li, X. Zhang, J.N. Hou, M. Xu, X.L. Lu, D.Z. Ma, B.K. Kim, Studies on thermally stimulated shape memory effect of segmented polyurethanes, J. Appl. Polym. Sci. 64 (8) (1997) 1511–1516.
[9] B.K. Kim, S.Y. Lee, M. Xu, Polyurethanes having shape memory effects, Polymer 37 (26) (1996) 5781–5793.
[10] M.F. Sonnenschein, Z. Lysenko, D.A. Brune, B.L. Wendt, A.K. Schrock, Enhancing polyurethane properties via soft segment crystallization, Polymer 46 (23) (2005) 10158–10166.
[11] X.H. Chen, Y.G. Liu, J.F. Li, T.W. Wong, T. Chen, T. Zhang, L. Wang, Light responsive self-healable carbon nanotube/polyurethane smart networks with precisely remote-controlled shape-changing properties, Polym. Test. 122 (2023).
[12] J.R. Lin, L.W. Chen, Study on shape-memory behavior of polyether-based polyurethanes. I. Influence of the hard-segment content, J. Appl. Polym. Sci. 69 (8) (1998) 1563–1574.
[13] F.K. Li, J.N. Hou, W. Zhu, X. Zhang, M. Xu, X.L. Luo, D.Z. Ma, B.K. Kim, Crystallinity and morphology of segmented polyurethanes with different soft-segment length, J. Appl. Polym. Sci. 62 (4) (1996) 631–638.
[14] J.F. Ban, D. Wu, J.Q. Liao, T.W. Xu, L.L. Pan, Evaluation of the performance of azobenzene liquid-crystal shape memory polyurethanes with photo-thermo-synergy responses, New J. Chem. 46 (26) (2022) 12808–12813.
[15] S. Park, J. Moon, B. Kim, M. Cho, Multi-scale coarse-grained molecular dynamics simulation to investigate the thermo-mechanical behavior of shape-memory polyurethane copolymers, Polymer 213 (2021).
[16] B.C. Abberton, W.K. Liu, S. Keten, Coarse-grained simulation of molecular mechanisms of recovery in thermally activated shape-memory polymers, J. Mech. Phys. Solid. 61 (12) (2013) 2625–2637.
[17] P. Nourian, C.D. Wick, G.Q. Li, A.J. Peters, Correlation between cyclic topology and shape memory properties of an amine-based thermoset shape memory polymer: a coarse-grained molecular dynamics study, Smart Mater. Struct. 31 (10) (2022).
[18] J.L. Hu, C.L. Zhang, X. Li, J.P. Han, F.L. Ji, Architectural evolution of phase domains in shape memory polyurethanes by dissipative particle dynamics simulations, Polym. Chem. 8 (1) (2017) 260–271.
[19] Y.R. Sliozberg, M. Kroger, T.C. Henry, S. Datta, B.D. Lawrence, A.J. Hall, A. Chattopadhyay, Computational design of shape memory polymer nanocomposites, Polymer 217 (2021).
[20] M.S. Uddin, J. Ju, Enhanced coarse-graining of thermoplastic polyurethane elastomer for multiscale modeling, J Eng Mater-T Asme 139 (1) (2017).
[21] Z.W. Cui, L.C. Brinson, Thermomechanical properties and deformation of coarse-grained models of hard-soft block copolymers, Phys. Rev. E 88 (2) (2013).
[22] J.L. Hu, C.L. Zhang, F.L. Ji, X. Li, J.P. Han, Y. Wu, Revealing the morphological architecture of a shape memory polyurethane by simulation, Sci Rep 6 (2016).
[23] Y. Wang, H.B. Wang, C.L. Li, S.Q. Sun, S.Q. Hu, CO-responsive Pickering emulsion stablized by modified silica nanoparticles: a dissipative particle dynamics simulation study, J. Ind. Eng. Chem. 97 (2021) 492–499.
[24] H. Mehralitabar, M. Taghdir, R. Mobasseri, H. Naderi-Manesh, The physicochemical properties role of a functionalized alkyl-peptide in nanofibre formation and neural progenitor cells viability and survival, Polym. Test. 91 (2020).
[25] T.K. Kwei, Phase-separation in segmented polyurethanes, J. Appl. Polym. Sci. 27 (8) (1982) 2891–2899.
[26] J.R. Zheng, R. Ozisik, R.W. Siegel, Phase separation and mechanical responses of polyurethane nanocomposites, Polymer 47 (22) (2006) 7786–7794.
[27] E. Yildirim, M. Yurtsever, G.L. Wilkes, I. Yilgör, Effect of intersegmental interactions on the morphology of segmented polyurethanes with mixed soft segments: a coarse-grained simulation study, Polymer 90 (2016) 204–214.
[28] Q.H. Meng, J.L. Hu, Y. Zhu, J. Lu, Y. Liu, Morphology, phase separation, thermal and mechanical property differences of shape memory fibres prepared by different spinning methods, Smart Mater. Struct. 16 (4) (2007) 1192–1197.
[29] H. Zhang, H.T. Wang, W. Zhong, Q.G. Du, A novel type of shape memory polymer blend and the shape memory mechanism, Polymer 50 (6) (2009) 1596–1601.
[30] M. Aldas, E. Rayón, J. López-Martínez, M.P. Arrieta, A deeper microscopic study of the interaction between gum rosin derivatives and a mater-Bi type bioplastic, Polym. Bull. (Heidelberg, Ger.) 12 (1) (2020).
[31] A. Saiani, C. Rochas, G. Eeckhaut, W.A. Daunch, J.W. Leenslag, J.S. Higgins, Origin of multiple melting endotherms in a high hard block content polyurethane. 2. Structural investigation, Macromolecules 37 (4) (2004) 1411–1421.
[32] M. Serrano, W.J. Macknight, E.L. Thomas, J.M. Ottino, Transport morphology relationships in segmented polybutadiene polyurethanes .1. Experimental results, Polymer 28 (10) (1987) 1667–1673.
[33] A. Saralegi, L. Rueda, B. Fernández-d'Arlas, I. Mondragon, A. Eceiza, M. A. Corcuera, Thermoplastic polyurethanes from renewable resources: effect of soft segment chemical structure and molecular weight on morphology and final properties, Polym. Int. 62 (1) (2013) 106–115.
[34] C.H.Y. Chentsai, E.L. Thomas, W.J. Macknight, N.S. Schneider, Structure and morphology of segmented polyurethanes .3. Electron-microscopy and small-angle X-ray-scattering studies of amorphous random segmented polyurethanes, Polymer 27 (5) (1986) 659–666.
[35] C.E. Wilkes, C.S. Yusek, Investigation of domain structure in urethan elastomers by X-ray and thermal methods, J. Macromol. Sci., Part B: Phys. 7 (1) (1973) 157–175.
[36] K. Park, W.H. Lim, E.A. Ko, H.S. Lee, Effect of molecular shape of diisocyanate units on the microscopic/macroscopic phase separation structure of polyurethanes, J. Polym. Sci., Polym. Phys. Ed. 49 (12) (2011) 890–897.
[37] A.A. Gavrilov, Y.V. Kudryavtsev, A.V. Chertovich, Phase diagrams of block copolymer melts by dissipative particle dynamics simulations, J. Chem. Phys. 139 (22) (2013).
[38] C. Li, S.L. Goodman, R.M. Albrecht, S.L. Cooper, Morphology of segmented polybutadiene polyurethane elastomers, Macromolecules 21 (8) (1988) 2367–2375.
[39] J.T. Koberstein, A.F. Galambos, L.M. Leung, Compression-molded polyurethane block copolymers .1. Microdomain morphology and thermomechanical properties, Macromolecules 25 (23) (1992) 6195–6204.
[40] S.B. Lin, K.S. Hwang, S.Y. Tsay, S.L. Cooper, Segmental orientation studies of polyether polyurethane block copolymers with different hard segment lengths and distributions, Colloid Polym. Sci. 263 (2) (1985) 128–140.
[41] F.L. Ji, J.L. Hu, T.C. Li, Y.W. Wong, Morphology and shape memory effect of segmented polyurethanes. Part I: with crystalline reversible phase, Polymer 48 (17) (2007) 5133–5145.
[42] R.D. Groot, P.B. Warren, Dissipative particle dynamics: bridging the gap between atomistic and mesoscopic simulation, J. Chem. Phys. 107 (11) (1997) 4423–4435.
[43] P. Espanol, P. Warren, Statistical-mechanics of dissipative particle dynamics, Europhys. Lett. 30 (4) (1995) 191–196.
[44] A. Maiti, S. McGrother, Bead-bead interaction parameters in dissipative particle dynamics: relation to bead-size, solubility parameter, and surface tension, J. Chem. Phys. 120 (3) (2004) 1594–1601.
[45] H. Sun, COMPASS: an ab initio force-field optimized for condensed-phase applications - overview with details on alkane and benzene compounds, J. Phys. Chem. B 102 (38) (1998) 7338–7364.
[46] H.C. Andersen, Molecular dynamics simulations at constant pressure and/or temperature, J. Chem. Phys. 72 (4) (1980) 2384–2393.
[47] H.J.C. Berendsen, J.P.M. Postma, W.F. Vangunsteren, A. Dinola, J.R. Haak, Molecular-dynamics with coupling to an external bath, J. Chem. Phys. 81 (8) (1984) 3684–3690.
[48] S. Sami, E. Yildirim, M. Yurtsever, E. Yurtsever, E. Yilgor, I. Yilgor, G.L. Wilkes, Understanding the influence of hydrogen bonding and diisocyanate symmetry on the morphology and properties of segmented polyurethanes and polyureas: computational and experimental study, Polymer 55 (18) (2014) 4563–4576.
[49] C. Danda, L.G. Amurin, P.A.R. Muñoz, D.A. Nagaoka, T. Schneider, B. Troxell, S. Khani, S.H. Domingues, R.J.E. Andrade, G.J.M. Fechine, J.M. Maia, Integrated computational and experimental design of ductile, abrasion-resistant thermoplastic polyurethane/graphene oxide nanocomposites, ACS Appl. Nano Mater. 3 (10) (2020) 9694–9705.

[50] F. Wang, Y.P. Ji, C.M. Chen, G.W. Zhang, Z.J. Chen, Tensile properties of 3D printed structures of polylactide with thermoplastic polyurethane, J. Polym. Res. 29 (8) (2022).
[51] R. Gallu, F. Méchin, F. Dalmas, J.F. Gérard, R. Perrin, F. Loup, On the use of solubility parameters to investigate phase separation-morphology-mechanical behavior relationships of TPU, Polymer 207 (2020).
[52] I. Yilgor, E. Yilgor, Silicone-Urea copolymers modified with polyethers, Sci. Techn. Silico. Silicone-Modified Mater. 964 (2007) 100–115.
[53] C.S. Schollenberger, K. Dinbergs, Thermoplastic polyurethane elastomer molecular weight-property relations - further-studies, J. Elastomers Plast. 11 (1) (1979) 58–91.
[54] C. Li, S.L. Cooper, Direct observation of the micromorphology of polyether polyurethanes using high-voltage electron-microscopy, Polymer 31 (1) (1990) 3–7.
[55] L.M. Leung, J.T. Koberstein, Small-angle scattering analysis of hard-microdomain structure and microphase mixing in polyurethane elastomers, J. Polym. Sci., Polym. Phys. Ed. 23 (9) (1985) 1883–1913.
[56] F.L. Ji, Study on the Shape Memory Mechanism of SMPUs and Development of High-Performance SMPUs, 2010.
[57] Y. Zheng, R. Dong, J. Shen, S. Guo, Tunable shape memory performances via multilayer assembly of thermoplastic polyurethane and polycaprolactone, ACS Appl. Mater. Interfaces 8 (2) (2016) 1371–1380.
[58] Y. Zheng, R. Dong, J. Shen, S. Guo, Strategy for fabricating multiple-shape-memory polymeric materials via the multilayer assembly of co-continuous blends, ACS Appl. Mater. Interfaces 9 (37) (2017) 32270–32279.
[59] Y. Zheng, J. Qin, J. Shen, S. Guo, Controllable distribution of conductive particles in polymer blends via a bilayer structure design: a strategy to fabricate shape-memory composites with tunable electro-responsive properties, J. Mater. Chem. C 8 (28) (2020) 9593–9601.
[60] Y.R. Sliozberg, J.L. Gair Jr., A.J. Hsieh, Dissipative particle dynamics simulation of microphase separation in polyurethane urea nanocomposites, Polymer 193 (2020) 122339.
[61] W.Y. Song, H. Lu, J.W. He, Z.J. Zhu, S.Y. He, D.H. Liu, .Y. Wang, Dynamics and morphology of self-assembly behavior of polymer-grafted nanoparticles: a dissipative particle dynamics simulation study, Polym. Int. 71 (11) (2022) 1330–1339.
[62] D. Sun Mai, L. Li, J. Zhou, Phase behavior of an amphiphilic block copolymer in ionic liquid: a dissipative particle dynamics study, J. Chem. Eng. Data 61 (12) (2016) 3998–4005.
[63] M. Kim, J. Moon, S. Park, M. Cho, Selective dissolution resistance control of EUV photoresist using multiscale simulation: rational design of hybrid system, Macromolecules 53 (12) (2020) 4748–4763.
[64] C.I. Huang, Y.J. Chiou, Y.K. Lan, Phase behavior of an amphiphilic molecule in the presence of two solvents by dissipative particle dynamics, Polymer 48 (2007) 877, 866.
[65] H. Liu, H. Qian, Y. Zhao, Z. Lu, Dissipative particle dynamics simulation study on the binary mixture phase separation coupled with polymerization, J. Chem. Phys. 127 (2007) 14.
[66] B. Zhou, W. Luo, J. Yang, X. Duan, Y. Wen, H. Zhou, R. Chen, B. Shan, Simulation of dispersion and alignment of carbon nanotubes in polymer flow using dissipative particle dynamics, Comput. Mater. Sci. 126 (2017) 35–42.
[67] S. Juan, C. Hua, C. Chen, X. Sun, H. Xi, Dissipative particle dynamics simulation of a gold nanoparticle system, Mol. Simulat. 31 (4) (2005) 277–282.
[68] S. Park, J. Moon, M. Cho, Y.S. Lee, H. Chung, S. Yang, Multiscale study of shape-memory behavior of semicrystalline polyurethane nanocomposites doped with silica nanoparticles based on coarse-grained molecular dynamics simulation, ACS Appl. Polym. Mater. 6 (6) (2024) 3192–3206.
[69] Z. Tongyang, X. Wang, Diffusion of rigid rodlike polymer in isotropic solutions studied by dissipative particle dynamics simulation, Polymer 54 (19) (2013) 5241–5249.
[70] Z. Tongyang, X. Wang, Dissipative particle dynamics study of translational diffusion of rigid-chain rodlike polymer in nematic phase, J. Chem. Phys. 139 (2013) 10.